| | |
|---|---|
| AUTHOR | Lucas Narciso, Tracy Ssali, Hidehiro Iida, Keith St Lawrence |
| TITLE | A non-invasive reference-based method for imaging the cerebral metabolic rate of oxygen by PET/MR: theory and error analysis |
| YEAR | 2021 |
| DOI | 10.1088/1361-6560/abe737 |
| VERSION | Author's accepted manuscript |
| CITATION | Lucas Narciso *et al* 2021 *Phys. Med. Biol.* **66** 065009 |

# 1 TITLE PAGE

## 1.1 TITLE

A non-invasive reference-based method for imaging the cerebral metabolic rate of oxygen by PET/MR: Theory and error analysis

## 1.2 AUTHORS NAMES AND AFFILIATIONS

Lucas Narciso [1,2], Tracy Ssali [1,2], Hidehiro Iida [3], Keith St Lawrence [1,2]

[1] Lawson Health Research Institute, London, Ontario, Canada

[2] Department of Medical Biophysics, Western University, London, Ontario, Canada

[3] University of Turku and Turku PET Centre, Turku, Finland

## 1.3 CORRESPONDING AUTHOR

Keith St Lawrence

Lawson Health Research Institute, 268 Grosvenor St., London, Ontario, N6A 4V2, Canada

Phone: +1-519-646-6100 x65737 E-mail address: kstlaw@lawsonimaging.ca

# 2 ABSTRACT AND KEYWORDS

## 2.1 UNSTRUCTURED ABSTRACT

Positron emission tomography (PET) remains the gold standard for quantitative imaging of the cerebral metabolic rate of oxygen ($CMRO_2$); however, it is an invasive and complex procedure that requires accounting for recirculating [$^{15}O$]$H_2O$ (RW) and the cerebral blood volume (CBV). This study presents a non-invasive reference-based technique for imaging $CMRO_2$ that was developed for PET/magnetic resonance imaging (MRI) with the goal of simplifying the PET procedure while maintaining its ability to quantify metabolism. The approach is to use whole-brain (WB) measurements of oxygen extraction fraction (OEF) and cerebral blood flow (CBF) to calibrate [$^{15}O$]$O_2$-PET data, thereby avoiding the need for invasive arterial sampling. Here we present the theoretical framework, along with error analyses, sensitivity to PET noise and inaccuracies in input parameters, and initial assessment on PET data acquired from healthy participants. Simulations showed that neglecting RW and CBV corrections caused errors in $CMRO_2$ of less than ± 10% for changes in regional OEF of ± 25%. These predictions were supported by applying the reference-based approach to PET data, which resulted in remarkably similar $CMRO_2$ images to those generated by analyzing the same data using a modelling approach that incorporated the

arterial input functions and corrected for CBV contributions. Significant correlations were observed between regional $CMRO_2$ values from the two techniques (slope = 1.00 ± 0.04, $R^2 > 0.98$) with no significant differences found for integration times of 3 and 5 min. In summary, results demonstrate the feasibility of producing quantitative $CMRO_2$ images by PET/MRI without the need for invasive blood sampling.

## 2.2 FIVE KEYWORDS

Cerebral blood flow, cerebral metabolic rate of oxygen, non-invasive PET, oxygen extraction fraction, PET/MRI

# 3 INTRODUCTION

One of the first applications of positron emission tomography (PET) was to measure the cerebral metabolic rate of oxygen ($CMRO_2$) using [$^{15}$O]-labelled tracers (Subramanyam *et al.*, 1978), driven by the recognition of the brain's high energy demands and continual adjustments to cerebral blood flow (CBF) to ensure sufficient supply of oxygen and glucose (Frackowiak *et al.*, 1980). A three-tracer method was developed using [$^{15}$O]oxygen to image the cerebral oxygen extraction fraction (OEF), [$^{15}$O]water to image CBF, and [$^{15}$O]carbon monoxide to correct for the activity originating from the cerebral blood volume (CBV) (Mintun *et al.*, 1984). In its autoradiographic form, this three-tracer method has been applied to many neurological diseases including cerebrovascular pathologies and neurodegenerative diseases (Baron and Jones, 2012). However, quantitative imaging $CMRO_2$ is a complex procedure requiring stable cerebral physiology for fairly long durations (30 to 60 min) due to the use of multiple tracers. Arterial blood sampling is required to measure the arterial input function (AIF) for each tracer, and plasma and red blood activity must be measured separately for [$^{15}$O]$O_2$ imaging to account for metabolically produced [$^{15}$O]$H_2O$ (Iida, Jones and Miura, 1993). Both recirculating water (RW) and blood-borne activity can cause substantial errors in the OEF and $CMRO_2$ estimates (Mintun *et al.*, 1984). Delay and

dispersion of the measured AIFs can also contribute to inaccurate measurements (Iida *et al.*, 1986, 1988; Kanno *et al.*, 1987; Meyer, 1989).

In an effort to reduce the length and complexity of the three-tracer method, Ohta *et al*. proposed a single [$^{15}$O]$O_2$ inhalation approach in which the imaging duration is restricted to less than 3 min to avoid substantial signal contributions from RW (Ohta *et al.*, 1992). The limitation with this method is the short imaging times can lead to poor counting statistics, although it performs just as accurately as the steady-state approach (Hattori *et al.*, 2004). Alternatively, Kudomi *et al*. proposed a rapid autoradiographic method based on sequential inhalation of [$^{15}$O]$CO_2$, [$^{15}$O]$O_2$, preceded by [$^{15}$O]CO (Kudomi *et al.*, 2005). In a more recent study, the total scan time was reduced to less than 10 min by introducing a novel approach for pixel-by-pixel calculation of four sets of kinetic parameters of $CMRO_2$, CBF, and functional vascular volumes for [$^{15}$O]$H_2O$ and [$^{15}$O]$O_2$, by means of a basis-function method in which the need for [$^{15}$O]CO inhalation can be eliminated (Kudomi *et al.*, 2013). Although separating the AIFs for the different $^{15}$O-tracers (Kudomi *et al.*, 2007) and correcting for RW can be incorporated into the mathematical model (Kudomi *et al.*, 2009), this method still requires arterial sampling for determining the whole blood AIF.

Magnetic resonance imaging (MRI) techniques based on the oxygen-dependent magnetic property of hemoglobin—i.e., blood oxygenation level dependent (BOLD)

contrast—have been proposed for imaging $CMRO_2$ (Yablonskiy, Sukstanskii and He, 2013). One approach is to combine estimates of local oxygen saturation obtained by quantitative BOLD (qBOLD) with CBF data from arterial spin labelling (ASL) (An *et al.*, 2001; He and Yablonskiy, 2007; Zhang *et al.*, 2017). Alternatively, calibrated BOLD, which was originally developed to measure activation-induced changes in oxidative metabolism, has been extended to estimate absolute $CMRO_2$ by using multiple calibration stimuli (Bulte *et al.*, 2012; Gauthier and Hoge, 2013; Merola *et al.*, 2018). Despite the advantages of an MRI-only method (i.e., non-invasive and no ionizing radiation), these approaches only provide indirect measures of tissue oxygenation since the BOLD signal must be isolated from other factors that affect signal decay (Blockley *et al.*, 2013).

This study presents a reference-based technique for imaging $CMRO_2$ that was developed specifically for hybrid PET/MRI to overcome some of the complexities associated with quantitative imaging of $CMRO_2$. The concept is to retain the fundamental advantage of $^{15}O_2$ PET in terms of directly measuring oxygen utilization, while incorporating complementary functional MRI techniques to provide a reference measurement for quantification. That is, whole brain (WB) CBF can be measured by phase-contrast MRI and venous oxygen saturation ($S_vO_2$) in the superior sagittal sinus measured by either susceptibility- or relaxation-based MRI oximetry—the combination of the two provides an

estimate of WB $CMRO_2$ (Lu and Ge, 2008; Jain, Langham and Wehrli, 2010; Wehrli *et al.*, 2014). These MR methods are fast, easy to implement, and most importantly can be acquired while collecting $^{15}O_2$ PET data (Barhoum *et al.*, 2015). The primary advantage of this hybrid imaging approach is it avoids invasive arterial blood sampling since WB $CMRO_2$ acts as a reference region. This is analogous to a previously published PET/MR approach for quantitative imaging of CBF by combining [$^{15}$O]water PET imaging with phase-contrast MRI (Ssali *et al.*, 2018). For imaging OEF and $CMRO_2$, a reference-region approach should also reduce the influence of RW and blood-borne activity, which are major sources of error with PET methods.

In this study, we present the theoretical framework for the proposed reference-based technique, as well as error analyses conducted to investigate the effects of neglecting RW and CBV contributions and inaccuracies in input parameters. The sensitivity of the reference-based method to statistical noise in the WB and local [$^{15}$O]$O_2$-PET time-activity curves (TACs) was also investigated. Finally, the feasibility of the reference-based method was evaluated by applying it to a human PET dataset consisting of [$^{15}$O]$O_2$, [$^{15}$O]$H_2O$ and [$^{15}$O]CO images. While this analysis precluded evaluating the accuracy of WB $CMRO_2$ from MR oximetry, it did provide the opportunity to evaluate the accuracy of the reference-based theory for imaging regional $CMRO_2$.

# 4 THEORY

$CMRO_2$ is defined as the product of CBF ($f$), OEF ($E$) and the arterial content of oxygen ($C_aO_2$):

$$CMRO_2 = E \cdot f \cdot C_aO_2 \quad (1)$$

where $C_aO_2 = 1.34 \cdot Hb \cdot S_aO_2 + 0.003 \cdot P_aO_2$. Each gram of hemoglobin can transport 1.34 mL of oxygen and the blood has $3x10^{-3}$ mL of dissolved oxygen per unit of arterial partial pressure of oxygen ($P_aO_2$) per 100 ml of blood. $C_aO_2$ is determined by measuring the hemoglobin concentration ($Hb$), $P_aO_2$ and arterial oxygen saturation ($S_aO_2$).

PET measurements of OEF are based on the one-compartment tissue model (Iida *et al.*, 2014), in which the rate of change in activity concentration for a given brain tissue ($C_b(t)$) is defined by the influx rate constant of $[^{15}O]O_2$ ($K_1^{O_2}$) across the BBB, the influx rate constant of metabolically generated $[^{15}O]H_2O$ ($K_1^{mH_2O}$), and the efflux rate constant of metabolically generated $[^{15}O]H_2O$ ($k_2^{mH_2O}$). A key assumption of the one-compartment model is that once $[^{15}O]O_2$ enters the brain it is immediately converted into $[^{15}O]H_2O$, and thus the efflux of $[^{15}O]O_2$ is negligible (Ohta *et al.*, 1992). The arterial activity concentration ($A_t(t)$) is given by the sum of the arterial activity concentration of $[^{15}O]O_2$ ($A_o(t)$) and RW

($A_w(t)$). The latter is generated by whole-body oxygen metabolism through the conversion of [$^{15}$O]$O_2$ to [$^{15}$O]$H_2O$.

## 4.1 SIMPLIFIED REFERENCE-BASED APPROACH

The reference-based imaging method is based on a simplified version of the one-compartment tissue model in which the RW contribution is neglected (i.e., $K_1^{mH_2O} \cdot A_w(t) \cong 0$) (Ohta *et al.*, 1992). The following differential equations are used to describe the time activity in the $i^{th}$ brain region/voxel ($C_i(t)$) and the whole brain ($C_{wb}(t)$):

$$\frac{dC_i(t)}{dt} = E_i \cdot f_i \cdot A_o(t) - \frac{f_i}{p} \cdot C_i(t) \tag{2}$$

$$\frac{dC_{wb}(t)}{dt} = E_{wb} \cdot f_{wb} \cdot A_o(t) - \frac{f_{wb}}{p} \cdot C_{wb}(t) \tag{3}$$

In these equations, the influx rate constant for [$^{15}$O]$O_2$ ($K_1^{O_2}$) is defined by $E \cdot f$ and efflux rate constant for metabolically generated [$^{15}$O]$H_2O$ ($k_2^{mH_2O}$) is $f/p$, where $p$ is the partition coefficient of water. By considering $A_o(t)$ to be the same for both WB and the $i^{th}$ brain region, the following expressions can be derived by integration:

$$\int_0^T \int_0^t A_o(u)du\,dt = \frac{\int_0^T C_{wb}(t)dt + \frac{f_{wb}}{p}\int_0^T \int_0^t C_{wb}(u)du\,dt}{E_{wb} \cdot f_{wb}} \tag{4}$$

$$\int_0^T \int_0^t A_o(u)du\,dt = \frac{\int_0^T C_i(t)dt + \frac{f_i}{p}\int_0^T \int_0^t C_i(u)du\,dt}{E_i \cdot f_i} \tag{5}$$

$$\frac{\int_0^T C_i(t)dt + \frac{f_i}{p}\int_0^T \int_0^t C_i(u)du\,dt}{E_i \cdot f_i} = \frac{\int_0^T C_{wb}(t)dt + \frac{f_{wb}}{p}\int_0^T \int_0^t C_{wb}(u)du\,dt}{E_{wb} \cdot f_{wb}} \tag{6}$$

Based on eq. (1), $CMRO_2$ in $i^{th}$ region can be defined by rearranging the terms:

$$CMRO_{2_i} = CMRO_{2_{wb}}\left[\frac{\int_0^T C_i(t)dt + \frac{f_i}{p}\int_0^T \int_0^t C_i(s)ds\,dt}{\int_0^T C_{wb}(t)dt + \frac{f_{wb}}{p}\int_0^T \int_0^t C_{wb}(s)ds\,dt}\right] \tag{7}$$

where $T$ is the PET scan time. Unlike standalone PET methods, calibration to a reference region also makes this approach less sensitive to RW and blood-borne activity since the method is only dependent on signal changes relative to WB TAC (Ohta *et al.*, 1992).

In a PET/MR experiment, the quantities $f_i$, $f_{wb}$ and $CMRO_{2_{wb}}$ can be measured by MRI: $f_i$ and $f_{wb}$ by ASL, and $CMRO_{2_{wb}}$ by combining $f_{wb}$ with an estimate of global venous oxygen saturation ($S_vO_2$) measured by MRI oximetry (Wehrli *et al.*, 2014).

## 4.2 RESIDUAL FUNCTIONS

The magnitude of error in $CMRO_{2_i}$ caused by neglecting RW and blood-borne activity can be estimated by deriving versions of eq. (7) that account for these signal contributions.

### 4.2.1 Recirculating water

The differential equations governing the time activity in brain tissue ($C_b(t)$) for both the $i^{th}$ region and WB can be modified to account for the influx of [$^{15}$O]$H_2O$:

$$\frac{d\,C_b(t)}{dt} = K_1^{O_2} \cdot A_o(t) + K_1^{mH_2O} \cdot A_w(t) - k_2^{mH_2O} \cdot C_b(t) \tag{8}$$

Following the same approach outlined through eqs. (4) to (6), the solution for $CMRO_{2_i}$ including the RW contribution is given by:

$$CMRO_{2_i} = CMRO_{2_{wb}} \left[ \frac{\int_0^T C_i(t)dt + \frac{f_i}{p}\int_0^T \int_0^t C_i(u)du\,dt}{\int_0^T C_{wb}(t)dt + \frac{f_{wb}}{p}\int_0^T \int_0^t C_{wb}(u)du\,dt} \right] + \varepsilon_{RW} \tag{9}$$

where $\varepsilon_{RW}$ is the RW residual function given by:

$$\varepsilon_{RW} = \frac{(E_i - E_{wb}) \cdot f_i \cdot f_{wb} \cdot C_a O_2}{\int_0^T C_{wb}(t)dt + \frac{f_{wb}}{p}\int_0^T \int_0^t C_{wb}(u)du\,dt} \int_0^T \int_0^t A_w(u)du\,dt \qquad (10)$$

### 4.2.2 Cerebral blood volume

The influence of blood-borne activity, which can cause significant overestimation of $CMRO_2$ in PET-only experiments (Lammertsma and Jones, 1983), can be accounted for by including vascular terms in the definition of the total measured activity:

$$C_{PET}(t) = (1 - CBV) \cdot C_b(t) + V_0^o \cdot A_o(t) + V_A^w \cdot A_w(t) \qquad (11)$$

where $V_0^o \cdot A_o(t)$ accounts for $[^{15}O]O_2$ bound to hemoglobin and $V_A^w \cdot A_w(t)$ accounts for arterial $[^{15}O]H_2O$. $V_A^w$ is the arterial blood volume, and $V_0^o = R_{Hct}(1 - EF_v) \cdot CBV$; $R_{Hct}$ is the small-to-large hematocrit ratio ($R_{Hct} = 0.85$) (Phelps *et al.*, 1979) and $F_v$ the venous-to-total blood volume ratio ($F_v = 0.835$) (Mintun *et al.*, 1984). The definition of $V_0^o$ reflects the fact that oxygen extraction primarily occurs at the capillary level (Mintun *et al.*, 1984). The expression for $CMRO_{2_i}$ including additional residue terms to account for the $[^{15}O]O_2$ and $[^{15}O]H_2O$ vascular contributions is given by:

$$CMRO_{2_i} = CMRO_{2_{wb}} \left[ \frac{\int_0^T C_i(t)dt + \frac{f_i}{p}\int_0^T \int_0^t C_i(u)du\,dt}{\int_0^T C_{wb}(t)dt + \frac{f_{wb}}{p}\int_0^T \int_0^t C_{wb}(u)du\,dt} \right] + \varepsilon_{V_0^o} + \varepsilon_{V_A^w} \tag{12}$$

$$\begin{aligned} \varepsilon_{V_0^o} = (1 - CBV_i)\frac{CMRO_{2_i}}{\alpha_{wb}}\left[\frac{CBV_i}{(1 - CBV_i)}\alpha_{wb} + V^o_{0_{wb}} \cdot \beta_{wb}\right] \\ - (1 - CBV_{wb})\frac{CMRO_{2_{wb}}}{\alpha_{wb}}\left[\frac{CBV_{wb}}{(1 - CBV_{wb})}\alpha_i + V^o_{0_i} \cdot \beta_i\right] \end{aligned} \tag{13}$$

$$\begin{aligned} \varepsilon_{V_A^w} = (1 - CBV_i)(1 - CBV_{wb})\left[\varepsilon_{RW} + \frac{V^w_{A_{wb}}}{1 - CBV_{wb}}\frac{CMRO_{2_i}}{\alpha_{wb}}\delta_{wb}\right. \\ \left. - \frac{V^w_{A_i}}{1 - CBV_i}\frac{CMRO_{2_{wb}}}{\alpha_{wb}}\delta_i\right] \end{aligned} \tag{14}$$

where $\alpha = \int_0^T C_b(t)dt + \frac{f}{p}\int_0^T \int_0^t C_b(u)du\,dt$, $\beta = \int_0^T A_o(t)dt + \frac{f}{p}\int_0^T \int_0^t A_o(u)du\,dt$, and $\delta = \int_0^T A_w(t)dt + \frac{f}{p}\int_0^T \int_0^t A_w(u)du\,dt$.

# 5 MATERIALS AND METHODS

## 5.1 SIMULATIONS

Simulations were conducted by generating theoretical versions of the total arterial input function, $A_t(t)$, and the recirculating water component, $A_w(t)$ (Herscovitch, Markham and Raichle, 1983; Kudomi *et al.*, 2009):

$$A_t(t) = \sum_{i=1}^{2} a_i \cdot t \cdot e^{-\frac{t}{b_i}} \tag{15}$$

where $a_1 = 100$, $a_2 = 1.2$, $b_1 = 0.3$ and $b_2 = 3$. Using the model proposed by Kudomi *et al*. (Kudomi *et al.*, 2009), $A_w(t)$ was derived from the total arterial curve:

$$A_w(t + \Delta t) = k\left(\alpha_1 \cdot A_t(t) \otimes e^{-\beta_1 t} + \alpha_2 \cdot A_t(t) \otimes e^{-\beta_2 t}\right) \tag{16}$$

where $\Delta t$ is the average delay of RW appearance for humans ($\Delta t$ = 20 s) (Iida, Jones and Miura, 1993), and $\alpha_{1,2}$ and $\beta_{1,2}$ are defined by three compartmental rate constants, $k$, $k_w$ and $k_2$. Average values from human studies for $k$, $k_w$ and $k_2$were selected: 0.13, 0.38 and 0.29 min$^{-1}$, respectively (Kudomi *et al.*, 2009). The AIF for [$^{15}$O]$O_2$ was given by $A_o(t) = A_t(t) - A_w(t)$. Simulated arterial input functions are presented in figure 1a. For illustration

purposes, figure 1b presents the corresponding simulated brain TACs generated for the three AIFs: [$^{15}$O]$O_2$-only ($C_{O_2}(t)$, eq.(2)), including RW ($C_{RW}(t)$, eq. (8)), including $V_0^o$ ($C_{CBV}(t)$, eq. (11)), and finally including RW, $V_0^o$ and $V_A^w$ ($C_{PET}(t)$, eq. (11)).

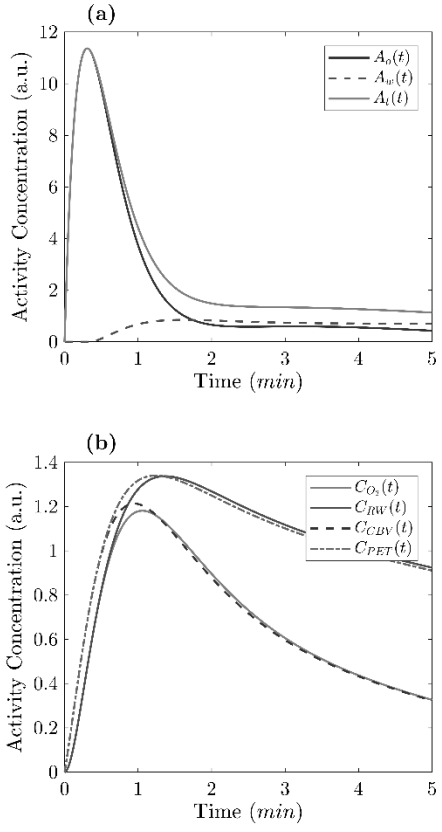


Figure 1. (a) Theoretical arterial input functions for [$^{15}$O]$O_2$ ($A_o(t)$, dark-grey line), metabolically generated [$^{15}$O]$H_2O$ ($A_w(t)$, dashed line), and their sum ($A_t(t)$, light-grey line). (b) Corresponding theoretical TACs for the three AIFs: [$^{15}$O]$O_2$-only (solid light-grey line), RW (solid dark-grey line), CBV ($V_0^o$, dashed dark-grey line), and both RW and CBV ($V_0^o$ and $V_A^w$, dash-dotted light-grey line).

In all cases, CBF = 50 mL (100g)$^{-1}$ min$^{-1}$, $p$ = 90 mL (100g)$^{-1}$, OEF = 0.40, CBV = 3.5 mL (100g)$^{-1}$, and $V_A^w$ = 1.5 mL (100g)$^{-1}$.

### 5.1.1 Error analysis

The error analysis focused on differences in hemodynamic and metabolic parameters between a given brain region and the WB as the influences of RW and blood-borne activity are only dependent on relative differences (i.e., between local and WB parameters as given by eqs. (10), (13) and (14)). The residue contributions from RW, eq. (10), and blood-borne activity, eqs. (13) and (14), were used to predict the magnitude of error in $CMRO_{2_i}$ when estimated from the simplified solution, eq. (7). Relative error, RE, was given by:

$$RE(\%) = 100\frac{\widehat{CMRO_{2_i}} - CMRO_{2_i}}{CMRO_{2_i}} = 100\frac{-\varepsilon_i}{CMRO_{2_i}} \quad (17)$$

where $\widehat{CMRO_{2_i}}$ and $CMRO_{2_i}$ are the predicted and true values, respectively. For all simulations, WB-CBF and WB-OEF were fixed to 50 mL (100g)$^{-1}$ min$^{-1}$ and 0.40, respectively. Likewise, WB-CBV = 3.5 mL (100g)$^{-1}$ and WB $V_A^w$ = 1.5 mL (100g)$^{-1}$. Changes in blood volume were modelled using the Grubb relationship: $CBV_i = CBV_{wb}(f_i/f_{wb})^{0.38}$ (Grubb *et al.*, 1974; Ito *et al.*, 2005). Finally, $CMRO_2$ was calculated

using eq. (1) with $C_aO_2$ = 0.175 $mLO_2$ $mL^{-1}$ ( $Hb$ = 13 g/mL, $S_aO_2$ = 98% and $P_aO_2$ = 90 mmHg).

Simulations were performed for three possible scenarios. First, assuming that OEF was uniform across the brain, as expected at rest in the healthy brain (i.e. $E_i = E_{wb} = 0.4$). The residues were calculated over a range of regional CBF (i.e., $f_i$ from 20 to 90 mL $(100g)^{-1}$ $min^{-1}$) and for integration time ($T$) ranging from 2 to 5 min. Next, $E_i$ was varied by ± 25% of WB-OEF (i.e., from 0.30 to 0.50), while constraining the corresponding $f_i$ using the relationship: $E_i = 1 - e^{-PS/f_i}$. $PS$ is the permeability-surface product for oxygen, which was fixed to 25 mL $(100g)^{-1}$ $min^{-1}$ based on normal values of OEF and CBF of 0.40 and 50 mL $(100g)^{-1}$ $min^{-1}$, respectively. Again, simulations were performed for values of $T$ ranging from 2 to 5 min.

The final set of simulations were performed by assuming a linear relationship between a change in regional CBF ($\Delta f_i$) and the corresponding change in $CMRO_2$ ($\Delta CMRO_{2_i}$), given by:

$$n = \left(\frac{\Delta f_i}{f_{wb}}\right)\left(\frac{\Delta CMRO_{2_i}}{CMRO_{2_{wb}}}\right)^{-1} \quad (18)$$

Values of $n$ equal to 1.3, 2 and 3 were considered in these simulations with a fixed integration time of 5 min (Sakoh *et al.*, 2000; Buxton *et al.*, 2004; Cooper *et al.*, 2011).

### 5.1.2 Errors in the input parameters

The impact of errors in the input parameter $f_i$ on local $CMRO_2$ was evaluated by generating simulated TACs for local CBF values of 20, 40, 60 and 80 mL $(100g)^{-1}$ $min^{-1}$ with whole-brain CBF fixed to 50 mL $(100g)^{-1}$ $min^{-1}$. These TACs were subsequently analyzed using eq. (7) with incorrect values of $f_i$ ranging from ± 20%. Given a PET/MRI experiment, these simulations are related to errors in the MRI measurements of local CBF. Note, a similar error analysis was not conducted for the other two input parameters, namely $f_{wb}$ and $E_{wb}$, since any error in either parameter will have an equivalent effect on both local and WB $CMRO_2$.

### 5.1.3 Noise contributions

Simulations were conducted to evaluate how noisy TACs impact the precision and accuracy of $CMRO_{2_i}$ estimates. Simulated TACs ($C_{O_2}(t)$) were generated using eq. (2) with Gaussian noise added to each time point as $C_{noisy}(t) = C_{O_2}(t) \cdot [1 + CV \cdot G(0,1)]$, where $CV$ is the coefficient of variation and $G(0,1)$ is a randomly generated number based on a Gaussian distribution of zero mean and standard deviation (SD) of one (Logan *et al.*, 2001;

Varga and Szabo, 2002). Since the magnitude of noise will be greater for local TACs, the $CV$ for the WB-TAC was fixed to 2%. This was based on comparing simulated noisy TACs to actual PET data, which are described in the next section. Simulations were performed for a range of flows from 10 to 100 mL (100g)$^{-1}$ min$^{-1}$, while local TACs were generated with $CV$ of 10%; and for local TACs generated with $CV$ ranging from 0 to 20%, while fixing true $CMRO_2$ to 3.5 mL$O_2$ (100g)$^{-1}$ min$^{-1}$ ( $f_i = f_{wb} =$ 50 mL (100g)$^{-1}$ min$^{-1}$ and $E_i = E_{wb} = 0.40$). The former was performed to evaluate how local $CMRO_2$ is affected by the noise, while the latter to investigate the error in local $CMRO_2$ for different levels of noise in the local TACs. Simulations were repeated twenty thousand times to obtain a distribution of $CMRO_2$ estimates.

## 5.2 APPLICATION OF THE REFERENCE-BASED APPROACH TO $^{15}$O-PET DATA

To demonstrate the feasibility of the reference-based method, it was applied to a dataset of $^{15}$O-PET images. This analysis required using WB-$CMRO_2$ estimates from PET instead of from MR oximetry. Consequently, the accuracy of MR oximetry could not be evaluated; however, the accuracy of regional $CMRO_2$ derived from eq. (7) was evaluated by comparison to $CMRO_2$ images obtained from the dual-tracer autoradiography (DARG) technique (Kudomi *et al.*, 2005).

Retrospective data from healthy volunteers ($n$ = 10, 23.2 ± 1.3 years, 64.3 ± 5.3 kg, 1 female) were acquired at the National Cerebral and Cardiovascular Center (Osaka, Japan). The imaging protocol used to generate the $CMRO_2$, CBF and OEF images from the DARG technique is described elsewhere (Kudomi *et al.*, 2013). Briefly, [$^{15}$O]$H_2O$ and [$^{15}$O]$O_2$ PET images were acquired with an ECAT-47 scanner (Siemens-CTI; 2D mode). Sequential [$^{15}$O]$O_2$ inhalation and [$^{15}$O]$H_2O$ injection lasted 8.5 min (~5 min [$^{15}$O]$O_2$ acquisition), while arterial blood was collected continuously with an AIF monitoring system (Kudomi *et al.*, 2003). A preceding [$^{15}$O]CO acquisition was used to correct for CBV. AIFs were delay and dispersion corrected, and RW was modeled by the method described by Kudomi *et al*. (Kudomi *et al.*, 2009). Images of OEF obtained from [$^{15}$O]$O_2$ PET data included corrections for RW and CBV contributions (Kudomi *et al.*, 2005).

Reference-based $CMRO_2$ images were generated from the TAC data by applying eq. (7) using an in-house MATLAB (2017b) script for integration times of 2, 3, 4, and 5 min. This analysis incorporated the CBF images acquired with [$^{15}$O]$H_2O$ and WB $CMRO_2$ was calculated from grey (GM) and white matter (WM) regions defined by segmenting $T_1$-weighted MRI images after removal of cerebrospinal voxels (SPM v.12, www.fil.ion.ucl.ac.uk/spm; 80% threshold).

All $CMRO_2$ images from the DARG and reference-based approaches were normalized to the MNI space. To compare the $CMRO_2$ images from the two methods, mean values were extracted for GM and WM regions, as well as regions of interest (ROIs) for frontal, occipital and temporal lobes, insula, hippocampus, precuneus, dorsal striatum and cerebellum. Correlation was evaluated in terms of the Pearson correlation coefficient ($\rho$). Statistical tests were performed using IBM SPSS Statistics (v. 26, https://www.ibm.com/analytics/spss-statistics-software).

# 6 RESULTS

Figure 2a shows the predicted error in regional $CMRO_2$ under the case of uniform OEF across the brain. In this scenario, the error is entirely due to regional variations in CBV (eqs. (13) and (14)) since the influence of RW is the same throughout the brain when $E_i = E_{wb}$ (see eq. (10)). Figure 2c-d show the predicted error in $CMRO_2$ when regional OEF was constrained to be inversely proportional to CBF. In this case, the error in $CMRO_2$ as a function of $E_i$ is presented for RW and CBV separately. The values of $E_i$ and $CMRO_{2_i}$ for a given $f_i$ are shown in figure 2b. Next, figure 3b shows the results of the simulations in which the value of $E_i$ was defined by eq. (18) (figure 3a); both RW and CBV were included and the integration time was fixed to 5 min.

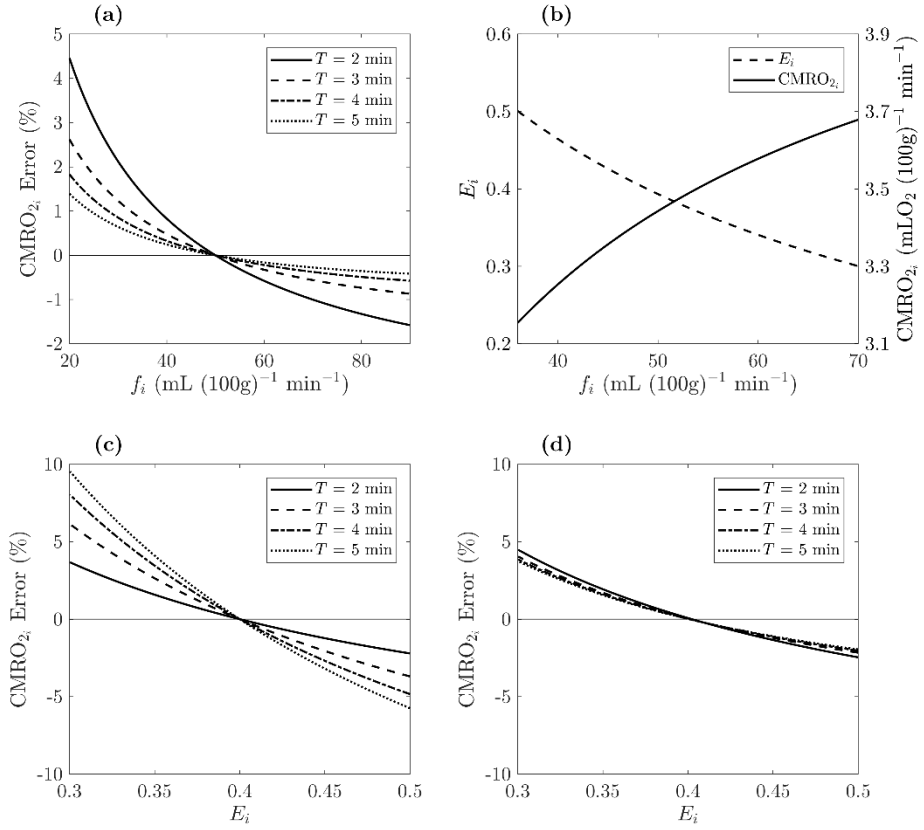


Figure 2. (a) Predicted error in local $CMRO_2$ from the reference-based approach as a function of local CBF when OEF is uniform across the brain. Simulations were generated for a fixed local OEF of 0.40 and for different acquisition times ($T$) ranging from 2 to 5 min. (b) Relationship between local CBF, OEF and $CMRO_2$ when $E_i = 1 - e^{-PS/f_i}$. Corresponding error in $CMRO_2$ as a function of $E_i$ is shown for neglecting (c) RW and (d) CBV. These errors were calculated using the residue functions given by eqs. (10), (13) and (14). WB values of CBF, OEF, CBV, and $V_A^w$ were fixed to 50 mL (100g)$^{-1}$ min$^{-1}$, 0.40, 3.5 mL (100g)$^{-1}$, and 1.5 mL (100g)$^{-1}$, respectively. Changes in blood volume were modelled using the Grubb relationship: $CBV_i = CBV_{wb}(f_i/f_{wb})^{0.38}$.

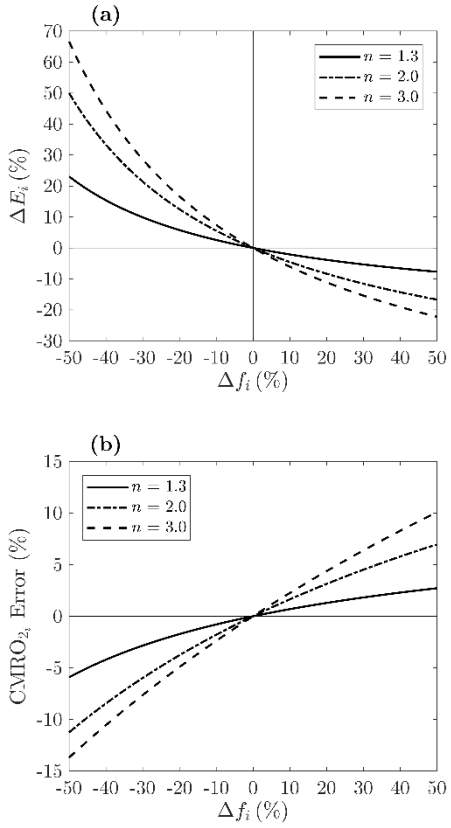


Figure 3. (a) Relative change in OEF ($\Delta E_i$) as a function of changes in CBF ($\Delta f_i$) for different values of $n$ (1.3, 2 and 3), which defines the relationship between $\Delta f_i$ and the corresponding change in $CMRO_2$ (eq. (18)). (b) Predicted error in $CMRO_2$ for changes in CBF from -50 to 50%. For all simulations: (i) Local $CMRO_2$ was determined by the reference-based approach (eq. (7)) and error obtained by residue functions (eqs. (10), (13) and (14)) with a 5 min integration; (ii) WB values of CBF, OEF, CBV, and $V_A^w$ were fixed to 50 mL $(100g)^{-1}$ $min^{-1}$, 0.40, 3.5 mL $(100g)^{-1}$, and 1.5 mL $(100g)^{-1}$, respectively; and (iii) Changes in blood volume were modelled using the Grubb relationship: $CBV_i = CBV_{wb}(f_i/f_{wb})^{0.38}$.

In terms of errors in the input parameters, figure 4 presents the predicted error in $CMRO_2$ when regional CBF was varied by ± 20% from its true value. The results for the different $f_i$ values demonstrated that the error in $CMRO_2$ increased with CBF, which was expected given that $f_i$ is a scaler in the numerator of eq. (7).

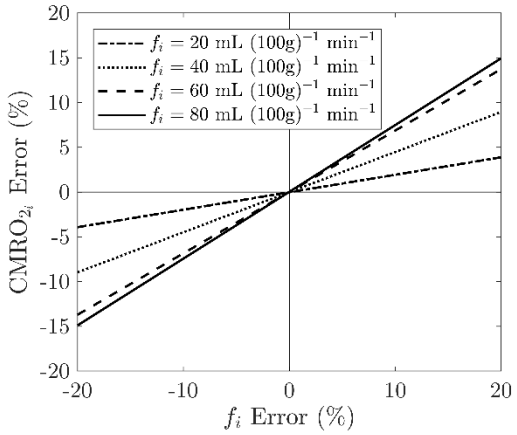


Figure 4. Error in the estimated $CMRO_2$ due to incorrectly measuring local CBF ($f_i$). Simulations were conducted for $f_i$ values ranging from 20 to 80 mL (100g)$^{-1}$ min$^{-1}$. For all simulations: (i) Local $CMRO_2$ was determined by the reference-based approach (eq. (7)) and error obtained by residue functions (eqs. (10), (13) and (14)), with a 5 min integration; (ii) WB values of CBF, OEF, CBV, and $V_A^w$ were fixed to 50 mL (100g)$^{-1}$ min$^{-1}$, 0.40, 3.5 mL (100g)$^{-1}$, and 1.5 mL (100g)$^{-1}$, respectively; and (iii) Changes in blood volume were modelled using the Grubb relationship: $CBV_i = CBV_{wb}(f_i/f_{wb})^{0.38}$.

The Monte Carlo simulations of noisy TACs indicated no bias in the $CMRO_2$ estimates across the different noise levels. figure 5a shows the predicted versus true $CMRO_2$ estimates when WB and local CV were 2% and 10%, respectively. Figure 5b presents the

error in $CMRO_2$ as a function of local CV. These results indicate that relatively small errors in the $CMRO_2$ estimates from the reference-based method (i.e. SD of ±1%) are expected for TAC noise levels up to a CV of 20%.

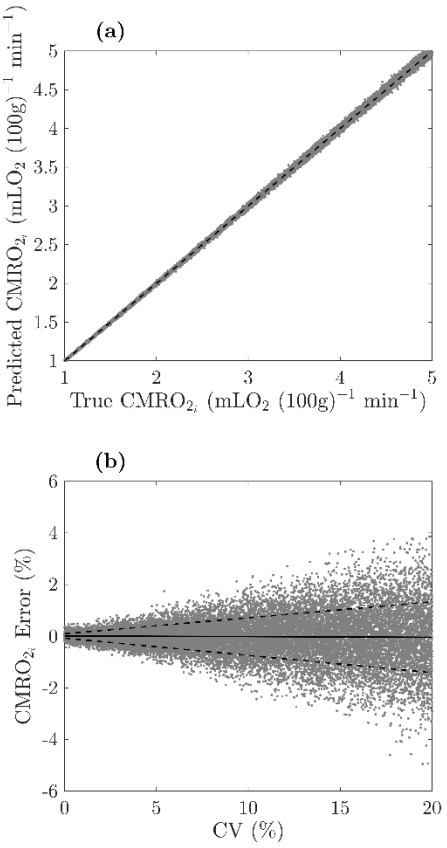


Figure 5. (a) Predicted versus true $CMRO_2$ after noise was added to WB (CV of 2%) and local (CV of 10%) TACs. The dashed black line is the identity line. (b) Error in $CMRO_2$ estimates after adding noise to local TACs (ranging from 0 to 20%, WB-TAC CV of 2%). True $CMRO_2$ was 3.5 $mLO_2$ $(100g)^{-1}$ $min^{-1}$ ($f_i = f_{wb} = 50$ mL $(100g)^{-1}$ $min^{-1}$ and $E_i = E_{wb} = 0.40$). Mean error is represented by the black solid line (± 1 SD, dashed black lines). For all simulations: (i) Local $CMRO_2$

was determined by the reference-based approach (eq. (7)) and error obtained by residue functions (eqs. (10), (13) and (14)), with a 5 min integration; (ii) WB values of CBF, OEF, CBV, and $V_A^w$ were fixed to 50 mL (100g)$^{-1}$ min$^{-1}$, 0.40, 3.5 mL (100g)$^{-1}$, and 1.5 mL (100g)$^{-1}$, respectively; and (iii) Changes in blood volume were modelled using the Grubb relationship: $CBV_i = CBV_{wb}(f_i/f_{wb})^{0.38}$.

The reference-based method produced similar $CMRO_2$ images (figure 6a and b; $T$ = 3 and 5 min, respectively) compared to those obtained with the DARG method (figure 6c). Mean $CMRO_2$ averaged across all brain voxels was 2.52 ± 0.85 $mLO_2$ (100g)$^{-1}$ min$^{-1}$ for the reference-based ($T$ = 5 min) and 2.51 ± 0.87 $mLO_2$ (100g)$^{-1}$ min$^{-1}$ for the DARG method ($p$ = 0.02). Figure 7a and b show OEF images from the reference-based approach ($T$ = 3 and 5 min, respectively), while figure 7c the DARG OEF images; OEF estimates were fairly uniform, as expected for the healthy brain. Voxel-wise average OEF was 0.39 ± 0.08 for the reference-based ($T$ = 5 min) 0.40 ± 0.09 for the DARG method ($p < 0.001$; 95% of the voxel-wise OEF values from the DARG technique were between 0.27 and 0.52). Figure 6d and figure 7d present images of the relative $CMRO_2$ and OEF differences between the two methods, which were 1.7 ± 14.5 and -1.3 ± 11.7 % for GM and WM $CMRO_2$, respectively; and -0.6 ± 10.1 and -2.9 ± 10.8 % for GM and WM OEF, respectively.

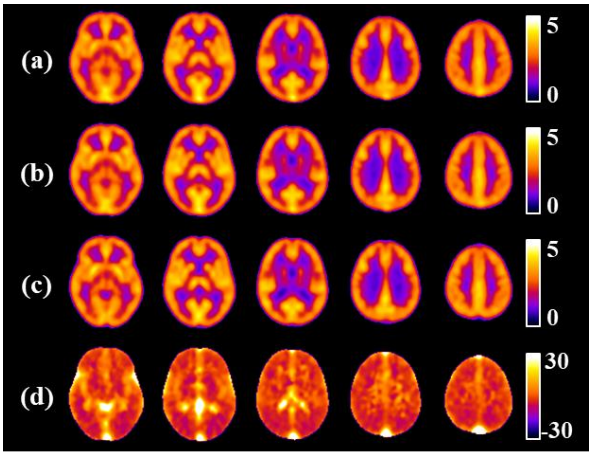


Figure 6. $CMRO_2$ images ($mLO_2$ $(100g)^{-1}$ $min^{-1}$) obtained with the reference-based method applied to [$^{15}$O]$O_2$-PET data from healthy volunteers ($n$ = 10) for integration times of 3 (a) and 5 min (b), compared to DARG images (c). (d) Images of the relative difference (%) between the 5-min reference-based and DARG $CMRO_2$ images. All images were normalized to the MNI space.

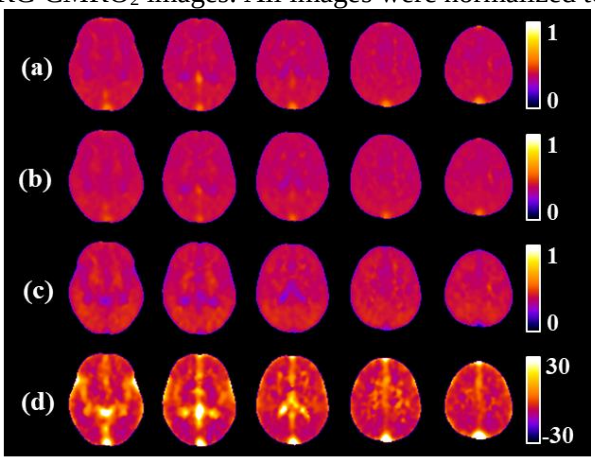


Figure 7. OEF images obtained with the reference-based method for integration times of 3 (a) and 5 min (b), compared to DARG images (c). (d) Images of the relative difference (%) between the 5-min reference-based and DARG OEF images. All images were normalized to the MNI space.

Significant correlation was found between regional $CMRO_2$ (figure 8a) and OEF (figure 8b) values from the reference-based and DARG methods for every ROI ($p < 0.001$; $R^2 > 0.98$; integration time of 5 min). Relative difference in $CMRO_2$ between the two methods plotted as a function of OEF is shown in figure 7c. To generate this figure, each subject's OEF values were normalized to WB-OEF and scaled to a mean value of 0.40. Mean $CMRO_2$ differences between reference-based (5 min integration time) and DARG measurements were 0.05 $mLO_2$ $(100g)^{-1}$ $min^{-1}$ for GM (1.7% higher, $p < 0.01$) and -0.04 $mLO_2$ $(100g)^{-1}$ $min^{-1}$ for WM (1.3% lower, $p < 0.01$).

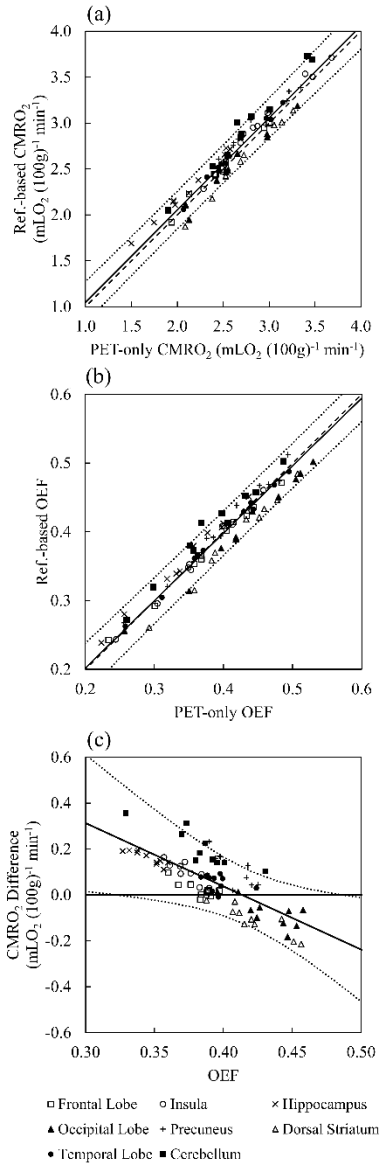


Figure 8. $CMRO_2$ (a) and OEF (b) estimates from DARG and reference-based methods ($n$ = 10; integration time of 5 min). Selected ROIs were frontal, occipital and temporal lobes, insula, hippocampus, precuneus, dorsal striatum, and cerebellum. The dashed line represents the identity line, while the solid black line is the average regression (average slope of $1.00 \pm 0.04$ and $0.98 \pm 0.04$ for $CMRO_2$ and OEF, respectively; average intercept of $0.04 \pm 0.14$ $mLO_2$ $(100g)^{-1}$ $min^{-1}$ and

0.01 ± 0.02 for $CMRO_2$ and OEF, respectively; $R^2 > 0.98$; 95% CIs are represented by the dotted lines). Significant correlation ($p < 0.001$) was observed for all ROIs, for both $CMRO_2$ and OEF. (c) Relative difference in $CMRO_2$ for the two methods plotted as a function of OEF. Each subject's OEF values were normalized to the WB extraction and scaled to OEF = 0.40. The solid black line is the average regression ($y = -2.75x + 1.14$; $R^2 = 0.63 \pm 0.23$; 95% CIs are represented by the dotted lines).

# 7 DISCUSSION

This study presents the derivation of a reference-based approach for imaging $CMRO_2$ developed to take advantage of simultaneous PET/MR imaging. The central concept is to use MRI to provide an independent estimate of WB $CMRO_2$ that can act as a reference in order to avoid invasive arterial sampling. The value of a reference region to simplify $^{15}O$-PET imaging was investigated by Ibaraki *et al*., although assumed values of WB CBF and OEF were required (Ibaraki *et al.*, 2004). Reference regions are also frequently used in PET studies of misery perfusion, although only to measure relative OEF (Jiang *et al.*, 2010). In addition to the model solution for the reference-based approach, this study also presents derivations of error terms that predict the effects of RW and blood-borne activity (i.e., CBV). The sensitivity of the method to errors in the input parameters and to statistical noise was investigated, the latter by Monte Carlo simulations; and an initial assessment of the approach was conducted using human PET data.

The value of the residual terms given in eqs. (10), (13) and (14) is they indicate which factors will contribute to errors due to neglecting signal contributions from RW and CBV. Eq. (10) shows that the magnitude of RW errors is proportional to the difference between regional and WB OEF, while eqs. (13) and (14) indicate that blood volume errors depend on regional differences in CBV and $CMRO_2$. Since $\varepsilon_{RW}$ depends on $A_w(t)$, its contribution will

increase with integration time as the concentration of metabolically generated [$^{15}$O]$H_2O$ builds. The time dependency of the CBV error is not as straightforward as $\varepsilon_{V_0^o}$ depends on $A_o(t)$ and $\varepsilon_{V_A^w}$ on $A_w(t)$. These differences are illustrated in figures 2 and 3. When $E_i = E_{wb}$, the error is primarily due to $\varepsilon_{V_0^o}$, which is heavily weighted towards the first pass of radiolabelled oxygen. Consequently, its signal contribution diminishes with integration time, reaching a minimum of ±1% for $T$ = 5 min (figure 2a). When regional OEF differs from the WB value, $\varepsilon_{RW}$ becomes the dominant residue and the error in regional $CMRO_2$ increases with integration time due to the greater contribution from RW. Figures 3 and 4 predict that the magnitude of the error will vary by approximately ± 10% when regional OEF varies from WB OEF by ± 25% (i.e., $0.3 \leq E_i \leq 0.5$ when $E_{wb} = 0.4$) depending on the integration time. To put this in context, 95% of the voxel-wise OEF values from the PET dataset were within the range from 0.27 to 0.52 (figure 7), which agrees with the general observation that OEF is fairly homogeneous in the healthy brain (Hattori *et al.*, 2004; Aanerud *et al.*, 2012; Kudomi *et al.*, 2013). The accuracy of the reference-based method is predicted to be worse for larger changes in regional OEF; for example, ischemic stroke can lead to compensatory increases in OEF as large as 50% (Pappata *et al.*, 1993). Figure 3 predicts an error of 15% for a 50% decrease in blood flow and a concomitant rise in OEF defined by $n$ = 3; however, as the flow-to-metabolism ratio increases (i.e., $n \to \infty$), so will the error in $CMRO_2$.

Shorter integration times would be the simplest approach for mitigating RW effects (Ohta *et al.*, 1992). An advantage of the reference-based method is that the procedure does not involve nonlinear optimization with multiple fitting parameters since $CMRO_2$ is determined directly from eq. (7). Integration times less than 5 min are feasible considering the noise simulations demonstrated that $CMRO_2$ estimates had an error $\leq$ 2% for TAC noise levels of up to 20% (figure 5). Alternatively, the accuracy of the reference-based approach could be improved by taking advantage of the known WB information and the measured TACs to directly model and correct for RW and CBV (Su *et al.*, 2017; Kudomi *et al.*, 2018) (currently under investigation).

In addition to $^{15}O$-related errors, the sensitivity of the $CMRO_2$ measurements to the input parameters was investigated. As evident by eq. (7), inaccurate WB $CMRO_2$ measurements will have an equal effect on regional $CMRO_2$ estimates. The results presented in figure 4 demonstrate that the approach also relies on accurately imaging CBF since the error in $CMRO_2$ is proportional to the error in the corresponding regional or voxel-wise CBF estimate. On a PET/MR scanner, non-invasive imaging of CBF with $[^{15}O]H_2O$ can be implemented by the approach recently proposed by Ssali *et al*. (Ssali *et al.*, 2018) Alternatively, the ability to acquire MR perfusion images simultaneously would reduce the PET procedure to just $[^{15}O]O_2$ inhalation, reducing the acquisition time to about five minutes.

Since both MRI oximetry and ASL are non-invasive and rapid methods, repeat measurements can be easily acquired to improve precision.

As an initial investigation of the reference-based method, it was applied to an existing PET dataset. While this application cannot address potential issues with the MR techniques, it did provide the opportunity to evaluate the influences of RW and the CBV. Figures 6 and 7 illustrate the similarity between $CMRO_2$ and OEF images generated from the reference-based approach for integration times of 3 and 5 min when compared to those from the previously validated DARG method. There were spatial differences, which are easier to identify in the difference images (figure 6d and figure 7d), with the largest occurring around the ventricles and large vessels, such as the superior sagittal sinus. Such large vascular artefacts are a consequence of neglecting blood-borne activity and they could be identified on a PET/MR scanner using non-contrast MR angiography/venography methods.

In terms of regional $CMRO_2$ and OEF, strong correlations ($p < 0.01$) were found between the two methods for all ROIs with an average regression slope of $1.00 \pm 0.04$ $mLO_2$ $(100g)^{-1}$ $min^{-1}$ for $CMRO_2$ and $0.98 \pm 0.04$ for OEF (figure 8a and b). $CMRO_2$ exhibited a dependency on integration time for the reference-based method. For the four regions (frontal and temporal lobes, precuneus and dorsal striatum), the $CMRO_2$ estimate converged to the corresponding value from DARG as T increased from 2 to 5 min;

while the opposite was observed in the other four ROIs. Based on the predictions of the residual terms, these patterns suggest the error was related to CBV for the first four ROIs and to RW for the remaining regions. To further investigate the agreement between the model predictions and the experimental results, the relative difference between the $CMRO_2$ estimates from the two methods was plotted as a function of OEF (integration time of 5 min; figure 8c). The deviation between the two methods was significantly correlated with the difference between the OEF for a given ROI and the WB value ($\rho$ = -0.80, $p < 0.001$). The magnitude of this difference as estimated from the regression analysis was similar to that predicted by the residuals (figure 2d).

In evaluating the potential sources of error with the proposed reference-based method, it is useful to compare it with other approaches developed to reduce the complexity of PET imaging of $CMRO_2$. These have included eliminating the need for measuring RW and CBV directly through modelling approaches (Ohta *et al.*, 1992; Iida, Jones and Miura, 1993; Kudomi *et al.*, 2009, 2013). However, they still require arterial sampling, which is technically complex, and the AIFs are inherently noisy. In an effort to circumvent this issue, newer methods have been developed based on measuring the image-derived input function (IDIF), either by PET alone (Kudomi *et al.*, 2016, 2018) or by incorporating structural MRI for guidance (Su *et al.*, 2013, 2017). However, reliably extracting the IDIF is challenging

due to the sensitivity to partial volume errors. Consequently, the accuracy of these methods relies on carefully measuring empirical scaling factors needed to quantify the IDIF.

# 8 CONCLUSIONS

This study presents an alternative approach that avoids the complications of measuring the input function altogether by calibrating the PET data with WB measurements, which can be accomplished by incorporating MRI measurements of OEF and CBF. When the method was applied to PET [$^{15}$O]$H_2O$ and [$^{15}$O]$O_2$ data from healthy individuals, the strong agreement with results derived with the DARG approach demonstrated the feasibility of the reference-based method in this population. Further studies are required to validate the reference-based approach in a PET/MR scanner and to investigate its feasibility in clinical studies, especially when local OEF varies significantly from WB extraction.

# 9 ACKNOWLEDGEMENTS

This work was supported by the Canadian Institutes of Health Research [grant 148600]. LN drafted the article and was responsible for the theory and analyses described in this paper. TS contributed with MATLAB scripts for the simulations, and data preprocessing and analysis. HI provided the human PET datasets and made substantial contributions to the theory and study design. TS, HI and KStL revised the manuscript critically for important intellectual content. KStL helped develop the theory and approved the final version to be published.

# 10 REFERENCES


Aanerud, J. *et al.* (2012) 'Brain energy metabolism and blood flow differences in healthy aging', *Journal of Cerebral Blood Flow and Metabolism*, 32(7), pp. 1177–1187. doi: 10.1038/jcbfm.2012.18.

An, H. *et al.* (2001) 'Quantitative measurements of cerebral metabolic rate of oxygen utilization using MRI: a volunteer study.', *NMR in Biomedicine*, 14(7–8), pp. 441–447. doi: 10.1002/nbm.717.

Barhoum, S. *et al.* (2015) 'Method for rapid MRI quantification of global cerebral metabolic rate of oxygen', *Journal of Cerebral Blood Flow & Metabolism*, 35(10), pp. 1616–1622. doi: 10.1038/jcbfm.2015.96.

Baron, J. C. and Jones, T. (2012) 'Oxygen metabolism, oxygen extraction and positron emission tomography: Historical perspective and impact on basic and clinical neuroscience', *NeuroImage*. Elsevier Inc., 61(2), pp. 492–504. doi: 10.1016/j.neuroimage.2011.12.036.

Blockley, N. P. *et al.* (2013) 'A review of calibrated blood oxygenation level-dependent (BOLD) methods for the measurement of task-induced changes in brain oxygen metabolism', *NMR in Biomedicine*, 26(8), pp. 987–1003. doi: 10.1002/nbm.2847.

Bulte, D. P. *et al.* (2012) 'Quantitative measurement of cerebral physiology using respiratory-calibrated MRI', *NeuroImage*. Elsevier Inc., 60(1), pp. 582–591. doi: 10.1016/j.neuroimage.2011.12.017.

Buxton, R. B. *et al.* (2004) 'Modeling the hemodynamic response to brain activation', *NeuroImage*, 23(SUPPL. 1), pp. 220–233. doi: 10.1016/j.neuroimage.2004.07.013.

Cooper, J. A. *et al.* (2011) 'Continuous monitoring of absolute cerebral blood flow by near-infrared spectroscopy during global and focal temporary vessel occlusion', *Journal of Applied Physiology*, 110(6), pp. 1691–1698. doi: 10.1152/japplphysiol.01458.2010.

Frackowiak, R. S. *et al.* (1980) 'Quantitative measurement of regional cerebral blood flow and oxygen metabolism in man using 15O and positron emission tomography: theory, procedure, and normal values.', *Journal of computer assisted tomography*, pp. 727–736.

Gauthier, C. J. and Hoge, R. D. (2013) 'A generalized procedure for calibrated MRI incorporating hyperoxia and hypercapnia', *Human Brain Mapping*, 34(5), pp. 1053–1069. doi: 10.1002/hbm.21495.

Grubb, R. L. *et al.* (1974) 'The fffects of changes in PaCO2 cerebral blood volume, blood flow, and vascular mean transit time', *Stroke*, 5(5), pp. 630–639. doi: 10.1161/01.STR.5.5.630.

Hattori, N. *et al.* (2004) ‘Accuracy of a method using short inhalation of (15)O-O(2) for measuring cerebral oxygen extraction fraction with PET in healthy humans.’, *Journal of nuclear medicine : official publication, Society of Nuclear Medicine*, 45(5), pp. 765–70. Available at: http://www.ncbi.nlm.nih.gov/pubmed/15136624 (Accessed: 29 October 2018).

He, X. and Yablonskiy, D. A. (2007) ‘Quantitative BOLD: Mapping of human cerebral deoxygenated blood volume and oxygen extraction fraction: Default state’, *Magnetic Resonance in Medicine*, 57(1), pp. 115–126. doi: 10.1002/mrm.21108.

Herscovitch, P., Markham, J. and Raichle, M. E. (1983) ‘Brain blood flow measured with intravenous H215O. I. Theory and error analysis’, *Journal of Nuclear Medicine*, 24(9), pp. 782–9. Available at: http://www.ncbi.nlm.nih.gov/pubmed/6604139.

Ibaraki, M. *et al.* (2004) ‘PET measurements of CBF, OEF, and CMRO2 without arterial sampling in hyperacute ischemic stroke: Method and error analysis’, *Annals of Nuclear Medicine*, 18(1), pp. 35–44. doi: 10.1007/BF02985612.

Iida, H. *et al.* (1986) ‘Error analysis of a quantitative cerebral blood flow measurement using H215O autoradiography and positron emission tomography, with respect to the dispersion of the input function’, *Journal of Cerebral Blood Flow & Metabolism*, 6(5), pp. 536–545. doi: 10.1038/jcbfm.1986.99.

Iida, H. *et al.* (1988) ‘Evaluation of regional differences of tracer appearance time in cerebral tissues using [15O]water and dynamic positron emission tomography’, *Journal of Cerebral Blood Flow and Metabolism*, 8(2), pp. 285–288. doi: 10.1038/jcbfm.1988.60.

Iida, H. *et al.* (2014) ‘Adequacy of a compartment model for CMRO2 quantitation using 15O-labeled oxygen and PET: a clearance measurement of 15O-radioactivity following intracarotid bolus injection of 15 O-labeled oxyhemoglobin on macaca fascicularis’, *Journal of Cerebral Blood Flow & Metabolism*, 34(10), pp. 1434–1439. doi: 10.1038/jcbfm.2014.118.

Iida, H., Jones, T. and Miura, S. (1993) ‘Modeling approach to eliminate the need to separate arterial plasma in oxygen-15 inhalation positron emission tomography’, *Journal of nuclear medicine : official publication, Society of Nuclear Medicine*, 34(8), pp. 1333–1340.

Ito, H. *et al.* (2005) ‘Changes in the arterial fraction of human cerebral blood volume during hypercapnia and hypocapnia measured by positron emission tomography’, *Journal of Cerebral Blood Flow and Metabolism*, 25(7), pp. 852–857. doi: 10.1038/sj.jcbfm.9600076.

Jain, V., Langham, M. C. and Wehrli, F. W. (2010) ‘MRI estimation of global brain oxygen consumption rate’, *Journal of Cerebral Blood Flow and Metabolism*. Nature

Publishing Group, 30(9), pp. 1598–1607. doi: 10.1038/jcbfm.2010.49.

Jiang, T. T. *et al.* (2010) 'Cerebellum as the normal reference for the detection of increased cerebral oxygen extraction', *Journal of Cerebral Blood Flow and Metabolism*. Nature Publishing Group, 30(10), pp. 1767–1776. doi: 10.1038/jcbfm.2010.43.

Kanno, I. *et al.* (1987) 'A system for cerebral blood flow measurement using an H215O autoradiographic method and positron emission tomography', *Journal of Cerebral Blood Flow and Metabolism*, 7(2), pp. 143–153. doi: 10.1038/jcbfm.1987.37.

Kudomi, N. *et al.* (2003) 'Development of a GSO detector assembly for a continuous blood sampling system', *IEEE Transactions on Nuclear Science*, 50(1), pp. 70–73. doi: 10.1109/TNS.2002.807869.

Kudomi, N. *et al.* (2005) 'Rapid quantitative measurement of CMRO2 and CBF by dual administration of 15O-labeled oxygen and water during a single PET scan - A validation study and error analysis in anesthetized monkeys', *Journal of Cerebral Blood Flow and Metabolism*, 25(9), pp. 1209–1224. doi: 10.1038/sj.jcbfm.9600118.

Kudomi, N. *et al.* (2007) 'Separation of input function for rapid measurement of quantitative CMRO2 and CBF in a single PET scan with a dual tracer administration method', *Physics in Medicine and Biology*, 52(7), pp. 1893–1908. doi: 10.1088/0031-

9155/52/7/009.

Kudomi, N. *et al.* (2009) ‘A physiologic model for recirculation water correction in CMRO2 assessment with 15O2 inhalation PET’, *Journal of Cerebral Blood Flow and Metabolism*, 29(2), pp. 355–364. doi: 10.1038/jcbfm.2008.132.

Kudomi, N. *et al.* (2013) ‘Rapid quantitative CBF and CMRO2 measurements from a single PET scan with sequential administration of dual 15O-labeled tracers’, *Journal of Cerebral Blood Flow and Metabolism*, 33(3), pp. 440–448. doi: 10.1038/jcbfm.2012.188.

Kudomi, N. *et al.* (2016) ‘Reconstruction of an input function from a dynamic PET water image using multiple tissue curves’, *Physics in Medicine and Biology*. IOP Publishing, 61(15), pp. 5755–5767. doi: 10.1088/0031-9155/61/15/5755.

Kudomi, N. *et al.* (2018) ‘Reconstruction of input functions from a dynamic PET image with sequential administration of 15O2 and H215O for noninvasive and ultra-rapid measurement of CBF, OEF, and CMRO2’, *Journal of Cerebral Blood Flow & Metabolism*, 38(5), pp. 780–792. doi: 10.1177/0271678X17713574.

Lammertsma, A. A. and Jones, T. (1983) ‘Correction for the presence of intravascular oxygen-15 in the steady-state technique for measuring regional oxygen extraction ratio in the brain: 1. Description of the method’, *Journal of Cerebral Blood Flow & Metabolism*,

3(4), pp. 416–424. doi: 10.1038/jcbfm.1983.67.

Logan, J. *et al.* (2001) ‘A strategy for removing the bias in the graphical analysis method’, *Journal of Cerebral Blood Flow and Metabolism*, 21(3), pp. 307–320. doi: 10.1097/00004647-200103000-00014.

Lu, H. and Ge, Y. (2008) ‘Quantitative evaluation of oxygenation in venous vessels using T2-relaxation-under-spin-tagging MRI’, *Magnetic Resonance in Medicine*, 60(2), pp. 357–363. doi: 10.1002/mrm.21627.

Merola, A. *et al.* (2018) ‘Assessing the repeatability of absolute CMRO2, OEF and haemodynamic measurements from calibrated fMRI’, *NeuroImage*. The Authors, 173(October 2017), pp. 113–126. doi: 10.1016/j.neuroimage.2018.02.020.

Meyer, E. (1989) ‘Simultaneous correction for tracer arrival delay and dispersion in CBF measurements by the H215O autoradiographic method and dynamic PET’, *Journal of nuclear medicine : official publication, Society of Nuclear Medicine*, 30(6), pp. 1069–78. Available at: http://www.ncbi.nlm.nih.gov/pubmed/2786948.

Mintun, M. A. *et al.* (1984) ‘Brain oxygen utilization measured with O-15 radiotracers and positron emission tomography’, *Journal of Nuclear Medicine*, 25(2), pp. 177–87. Available at: http://www.ncbi.nlm.nih.gov/pubmed/6610032.

Ohta, S. *et al.* (1992) 'Oxygen consumption of the living human brain measured after a single inhalation of positron emitting oxygen', *Journal of Cerebral Blood Flow and Metabolism*, 12(2), pp. 179–192. doi: 10.1038/jcbfm.1992.28.

Pappata, S. *et al.* (1993) 'PET study of changes in local brain hemodynamics and oxygen metabolism after unilateral middle cerebral artery occlusion in baboons', *Journal of Cerebral Blood Flow and Metabolism*, 13(3), pp. 416–424. doi: 10.1038/jcbfm.1993.56.

Phelps, M. E. *et al.* (1979) 'Validation of tomographic measurement of cerebral blood volume with C-11-labeled carboxyhemoglobin.', *Journal of nuclear medicine : official publication, Society of Nuclear Medicine*, 20(4), pp. 328–34. Available at: http://www.ncbi.nlm.nih.gov/pubmed/119833.

Sakoh, M. *et al.* (2000) 'Relationship between residual cerebral blood flow and oxygen metabolism as predictive of ischemic tissue viability: sequential multitracer positron emission tomography scanning of middle cerebral artery occlusion during the critical first 6 hours after st', *Journal of Neurosurgery*, 93(4), pp. 647–657. doi: 10.3171/jns.2000.93.4.0647.

Ssali, T. *et al.* (2018) 'A noninvasive method for quantifying cerebral blood flow by hybrid PET/MRI', *Journal of Nuclear Medicine*, 59(8), pp. 1329–1334. doi:

10.2967/jnumed.117.203414.

Su, Y. *et al.* (2013) ‘Noninvasive estimation of the arterial input function in positron emission tomography imaging of cerebral blood flow’, *Journal of Cerebral Blood Flow and Metabolism*, 33(1), pp. 115–121. doi: 10.1038/jcbfm.2012.143.

Su, Y. *et al.* (2017) ‘Quantitative hemodynamic PET imaging using image-derived arterial input function and a PET/MR hybrid scanner’, *Journal of Cerebral Blood Flow and Metabolism*, 37(4), pp. 1435–1446. doi: 10.1177/0271678X16656200.

Subramanyam, R. *et al.* (1978) ‘A model for regional cerebral oxygen distribution during continuous inhalation of 15O2, C15O, and C15O2’, *Journal of nuclear medicine : official publication, Society of Nuclear Medicine*, 19(1), pp. 48–53. Available at: http://www.ncbi.nlm.nih.gov/pubmed/621563.

Varga, J. and Szabo, Z. (2002) ‘Modified regression model for the Logan plot’, *Journal of Cerebral Blood Flow and Metabolism*, 22(2), pp. 240–244. doi: 10.1097/00004647-200202000-00012.

Wehrli, F. W. *et al.* (2014) ‘Time-resolved MRI oximetry for quantifying CMRO2 and vascular reactivity’, *Academic Radiology*, 21(2), pp. 207–214. doi: 10.1016/j.acra.2013.11.001.

Yablonskiy, D. A., Sukstanskii, A. L. and He, X. (2013) 'Blood oxygenation level-dependent (BOLD)-based techniques for the quantification of brain hemodynamic and metabolic properties - theoretical models and experimental approaches', *NMR in Biomedicine*, 26(8), pp. 963–986. doi: 10.1002/nbm.2839.

Zhang, J. *et al.* (2017) 'Cerebral metabolic rate of oxygen (CMRO2) mapping with hyperventilation challenge using quantitative susceptibility mapping (QSM)', *Magnetic Resonance in Medicine*, 77(5), pp. 1762–1773. doi: 10.1002/mrm.26253.